MCB
Journals.ASM.org

MCJ/DnaJC15, an Endogenous Mitochondrial Repressor of the Respiratory Chain That Controls Metabolic Alterations

Ketki M. Hatle,[a]* Phani Gummadidala,[a] Nicolás Navasa,[b,c] Edgar Bernardo,[a] John Dodge,[a] Brian Silverstrim,[a] Karen Fortner,[a] Elianne Burg,[d] Benajamin T. Suratt,[d] Juergen Hammer,[e] Michael Radermacher,[f] Douglas J. Taatjes,[g] Tina Thornton,[a] Juan Anguita,[b,c,h] Mercedes Rincon[a]

Department of Medicine, Division of Immunobiology,[a] Department of Medicine, Pulmonary and Critical Care Unit,[d] Department of Molecular Physiology and Biophysics,[f] and Department of Pathology,[g] University of Vermont, Burlington, Vermont, USA; Department of Veterinary and Animal Sciences, University of Massachusetts Amherst, Amherst, Massachusetts, USA[b]; CIC bioGUNE, Proteomics Unit, Derio, Bizkaia, Spain[c]; Ikerbasque Foundation, Bilbao, Bizkaia, Spain[h]; Hoffmann-La Roche Inc., Pharma Research Early Development Informatics, Nutley, New Jersey, USA[e]

Mitochondria are the main engine that generates ATP through oxidative phosphorylation within the respiratory chain. Mitochondrial respiration is regulated according to the metabolic needs of cells and can be modulated in response to metabolic changes. Little is known about the mechanisms that regulate this process. Here, we identify MCJ/DnaJC15 as a distinct cochaperone that localizes at the mitochondrial inner membrane, where it interacts preferentially with complex I of the electron transfer chain. We show that MCJ impairs the formation of supercomplexes and functions as a negative regulator of the respiratory chain. The loss of MCJ leads to increased complex I activity, mitochondrial membrane potential, and ATP production. Although MCJ is dispensable for mitochondrial function under normal physiological conditions, MCJ deficiency affects the pathophysiology resulting from metabolic alterations. Thus, enhanced mitochondrial respiration in the absence of MCJ prevents the pathological accumulation of lipids in the liver in response to both fasting and a high-cholesterol diet. Impaired expression or loss of MCJ expression may therefore result in a "rapid" metabolism that mitigates the consequences of metabolic disorders.

Mitochondria are essential organelles for eukaryotic cells due to their role in controlling cell metabolism. Mitochondria are the main source of ATP in most cells. ATP is generated through oxidative phosphorylation that is mediated by the mitochondrial respiratory chain (electron transfer chain [ETC]). Four respiratory protein complexes constitute the mitochondrial ETC. Complex I is a multisubunit complex (49 subunits) that has NADH-ubiquinone oxidoreductase activity. Complex II mediates succinate dehydrogenase activity. Complex III is a ubiquinol-cytochrome *c* reductase, while complex IV has cytochrome *c* oxidase activity. The electrons resulting from the oxidative process are transferred from complex I and complex II to complex III through ubiquinone and from complex III to complex IV through cytochrome *c* as shuttles. The transfer of electrons from complexes I, III, and IV is coupled to the transport of H^+ across the mitochondrial inner membrane and H^+ accumulation in the intermembrane space that generates a mitochondrial membrane potential (MMP) relative to the mitochondrial matrix. This electrochemical proton gradient is used by complex V (ATP synthase) of the respiratory chain to generate ATP from ADP with the released energy as H^+ flowing back into the mitochondrial matrix. Thus, the transport of H^+ from the different complexes and generation of MMP are key for ATP synthesis by mitochondria. While electron transfer among complexes of the respiratory chain is highly efficient due to the use of specific shuttles, some electrons may escape and lead to the generation of reactive oxygen species (ROS) as a by-product (1). Initial studies in bacteria and yeast, together with more recent studies in mammals, have revealed the presence of mitochondrial supercomplexes that contain one or more units of the respiratory chain complexes (2–4). In mammalian cells, supercomplexes containing complexes I, III, and IV have been characterized and defined as "respirasomes" (5, 6). The functions of the supercomplexes are likely to facilitate the transfer of electrons between complexes and to minimize the risk of releasing electrons. Recent studies have reported mechanisms that regulate the assembly of these supercomplexes (7–9). Less is known about mechanisms that regulate the activities of the individual complexes or the formation of supercomplexes according to the metabolic needs of cells.

Under aerobic conditions, mitochondria are the main source of energy for most cells, with the exception of cancer cells, which switch to aerobic glycolysis instead of oxidative phosphorylation, a phenomenon defined as the Warburg effect (10, 11). Highly metabolic tissues, such as heart, liver, skeletal muscle, or kidney, have a larger content of mitochondria. Under physiological conditions, the functional quality of mitochondria is maintained through a balance of biogenesis and autophagy destruction that mediates the periodic (around 17 days) turnover of the mitochondria (12). However, other mechanisms should contribute to the regulation of the mitochondrial respiratory chain according to needs in response to acute or chronic metabolic changes. Since high turnover of mitochondria can affect the life span of cells, the presence of alternative mechanisms that can rapidly regulate mitochondrial respiration would be beneficial to the cells. Fasting, caloric restrictions, overfeeding (obesity), hyperglycemia, hyper-

Received 11 February 2013 **Returned for modification** 28 February 2013
Accepted 20 March 2013
Published ahead of print 25 March 2013
Address correspondence to Mercedes Rincon, mercedes.rincon@uvm.edu.
* Present address: Ketki M. Hatle, Department of Cell Biology, Harvard Medical School, Boston, Massachusetts, USA.

doi:10.1128/MCB.00189-13

cholesterolemia, and hypoxia are some of the metabolic alterations that can affect mitochondrial function. Several proteins have been shown to be associated with and contribute to the activity of ETC complexes (e.g., GRIM-19, Rcf1, and STAT3) (7, 9, 13–15). Less is known about the presence of inhibitory mechanisms for the regulation of the ETC. Here, we describe the expression and function of MCJ (methylation-controlled J protein) as a negative regulator of ETC that plays a role in mitochondrial function in response to altered metabolic conditions.

MCJ/DnaJC15 is a member of the DnaJC subfamily of cochaperones. MCJ was first reported in human ovarian cancer cell lines, where *mcj* gene expression was found to be negatively regulated by methylation of CpG islands within the promoter and first exon/intron sequences (16, 17). Methylation of *mcj* gene CpG islands has also been reported in ovarian cancer, Wilms' tumors, malignant brain tumors, and melanoma (18–21). MCJ is a small protein of 147 amino acids (aa) and a unique member of the DnaJC family. It contains a J domain located at the C terminus, as opposed to the common N-terminal position, and its N-terminal region has no homology with any other known protein. In addition, MCJ also contains a transmembrane domain, while most DnaJ proteins are soluble. A number of studies have examined the methylation status of the *mcj* gene in malignant cells, yet little is known about the function of the protein. MCJ expression does not seem to affect the proliferation of ovarian cancer cells, but overexpression of MCJ increases their sensitivity to cisplatin and vincristine (16, 22). Moreover, a study examining *mcj* gene methylation in ovarian cancer patients has shown that the presence of high levels of CpG island methylation in the *mcj* gene (associated with loss of MCJ gene expression) correlates with a diminished response to chemotherapy and poor survival (20). MCJ is also expressed in breast and uterine cancer cells that are sensitive to different chemotherapeutic drugs but not in multidrug-resistant cancer cells (23). Inhibition of MCJ expression in drug-sensitive breast cancer cell lines causes an increased 50% lethal dose (LD_{50}) for specific chemotherapeutic drugs (e.g., doxorubicin and paclitaxel) (23). The *in vivo* expression and function of this cochaperone in normal tissues remain unknown.

Here, we identify the mouse ortholog of MCJ and show that MCJ resides in the mitochondria, where it associates with and negatively regulates complex I of the mitochondrial respiratory chain. MCJ interferes with the formation of ETC supercomplexes. Loss of MCJ leads to increased complex I activity, hyperpolarization of mitochondria, and increased generation of ATP. While under normal physiological conditions MCJ is dispensable, enhanced mitochondrial respiration in the absence of MCJ prevents the pathological accumulation of lipids in the liver under altered metabolic conditions, such as fasting and a high-cholesterol diet. Thus, MCJ is an essential negative regulator of mitochondrial metabolism.

MATERIALS AND METHODS

Mice. C57BL/6J mice were purchased from Jackson Laboratories. MCJ-targeted embryonic stem (ES) cells (RRN 226) were obtained from Baygenomics. The gene-trapped ES cells were injected into C57BL/6J blastocysts and implanted in pseudopregnant females at the University of Vermont Transgenic Mouse Facility. Six male chimeras were obtained, with 5 showing more than 95% chimerism. The chimeras were crossed with C57BL/6J females, and all of them led to germ line transmission (100%). The mice were further backcrossed with C57BL/6 mice for at least 7 generations. The heterozygous males and females were crossed for the generation of MCJ homozygous knockout (KO). The mice were used between 10 and 14 weeks of age. For the fasting studies, the mice were kept with water but not food for 36 h. For liver cholesterol accumulation, the mice were kept on a high-cholesterol diet (Harlan Teklad TD.902221) for 4 weeks, as we previously described (24). All mice were housed under pathogen-free conditions at the animal care facility at the University of Vermont. The procedures were approved by the University of Vermont Institutional Animal Care and Use Committee.

Cell preparation, culture conditions, proliferation, and reagents. CD8 T cells and CD4 T cells were purified from spleen and lymph nodes by negative selection, as previously described (25, 26), and by positive selection using the MACS system, as recommended by the manufacturer (Miltenyi). MCF7 and MCF7/siMCJ cell lines were maintained as previously described (23). Rotenone (used at 10 μM) was purchased from Sigma.

Northern blot analysis. Human and mouse multiple-tissue Northern blots (MTN) were purchased from Clontech Laboratories, Inc., CA, and contained normalized levels of poly(A) RNA from different tissues. Radiolabeling of both mouse and human MCJ probes was performed as described previously (27), and Northern blot analysis was done according to the manufacturer's instructions.

Southern blot analysis. Ten micrograms of tail genomic DNA digested with NcoI was separated in an agarose gel, transferred onto a Hybond nylon membrane, radiolabeled, and probed with a PCR-amplified region from MCJ intron 1 (5′-GTGGGGGTGTCTGTGAAGTAGTTT-3′ and 5′-CTGGGATTTAAGGAGTTCACAA-3′).

RNA isolation and RT-PCR. Total RNA was isolated using the Qiagen mini RNeasy kit, as recommended by the manufacturer. The first-strand cDNA was obtained by reverse transcription as described previously (23). cDNA was used to detect mouse hypoxanthine phosphoribosyltransferase (HPRT), MCJ, and β_2 microglobulin by conventional PCR or real-time reverse transcriptase PCR (RT-PCR). For the real-time RT-PCR analysis (Applied Biosystems), the following designed set of primers and probe was used for mouse MCJ (forward, 5′-CCG AAT ACC TGC CTC CTT CTG-3′; reverse, 5′-ACA CAG CGG GGA GAA GGT T-3′; probe, 5′-CCA AAG GTC GGA CGC CGA CAT C-3′). The relative values were determined by the comparative cycle threshold (CT) analysis method using HPRT or β_2 microglobulin as a housekeeping gene. Conventional RT-PCR amplification of *MCJ* was done using the following primers: 5′-AAG TAA TCA CGG CAA CAG CAA GG-3′ and 5′-AAT AAA AGC CTG GCA GCC TTG C-3′.

Western blot analysis. Whole-cell extracts were prepared in Triton lysis buffer, as previously described (23). Mitochondrial and cytosolic extracts were purified using the cell fractionation kit-standard (MitoSciences) for CD8 T cells and MCF7 cells or the Mitochondrial Fractionation Kit (Active Motif) for tissues. Mitochondrial extracts were solubilized with either lauryl maltoside (1%) or digitonin (2%) when specified. Isolation of the mitochondrial inner membrane fraction was performed as previously described (28) using purified mitochondrial extracts from the heart. Western blot analyses were performed as previously described (23). The anti-mouse MCJ rabbit polyclonal antibody (Ab) was generated by immunization with the N-terminal peptide (35 aa) of mouse MCJ. Rabbit serum polyclonal Ab underwent affinity immunopurification (Cocalico Biologicals, Inc.). The anti-human MCJ mouse monoclonal Ab (BioMosaics) has been described previously (23). Other antibodies used were antiactin, anti-glyceraldehyde-3-phosphate dehydrogenase (anti-GAPDH), anti-rabbit IgG, and anti-goat IgG (Santa Cruz Biotechnology); anti-mouse IgG (Jackson Immunologicals); anti-CoxIV (Cell Signaling); anti-NDUFA9, anti-NDUFS3, and complex III Core1 protein (MitoSciences); anti-glycogen synthase (Cell Signaling); anti-phosphoenolpyruvate carboxykinase (anti-PEPCK) (Santa Cruz); calreticulin (Enzo Life Science); and sintaxin 11 (BD Bioscience). The LumiGlo chemiluminescent substrate system (KPL, Maryland) was used to visualize the proteins. Immunoprecipitations of complex I and complex III were performed using mitochondrial extracts generated as described above and

solubilized with maltoside (1%) as the detergent and the complex I or complex III Immunocapture monoclonal antibody (MitoSciences) as recommended by the manufacturer. The immunoprecipitates were then examined for the presence of MCJ, or specific subunits were examined for complex I, III, or IV subunits by Western blotting.

Blue native (BN) PAGE. Purified mitochondria were solubilized in native PAGE loading buffer (Invitrogen) containing 2% digitonin (Sigma). When specified, maltoside was also used for solubilization. Complexes were resolved by electrophoresis through 4 to 16% NativePAGE Novex Bis-Tris gels (Invitrogen). Lanes were excised for second-dimension (2D) SDS-PAGE, followed by transfer to a polyvinylidene difluoride (PVDF) membrane for Western blot analysis. In gel complex I, activity assays were performed as previously described (29) by incubating excised lane strips in 5 mM Tris-HCl, pH.7.4, 0.1 mg/ml NADH (Sigma), and 2.5 mg/ml Nitro Blue Tetrazolium (Sigma). Protein complexes were visualized by Coomassie blue (Sigma) staining. Protein elution was performed by incubating the excised gel piece with 0.1% digitonin for 4 h.

Flow cytometry analysis. Mitochondrial membrane potential analysis was performed by staining with TMRE (Molecular Probes; 1 μM) for 20 min at 37°C as recommended by the manufacturer. Mitochondrial ROS analysis was performed by staining with MitoSox-Red (Invitrogen; 2.5 μM) for 10 min at 37°C, as recommended by the manufacturer. All samples were examined by flow cytometry analysis using an LSRII flow cytometer (BD Biosciences) and Flowjo software. For MCJ mRNA expression, CD4 T cells, CD8 T cells, and B cells were purified from spleen and lymph nodes by immunostaining for CD4, CD8, and B220 (B cell marker) and flow cytometry cell sorting (FACSAria flow cell sorter; BD Bioscience).

Confocal microscopy analysis. Cell preparation and immunostaining of transfected 293T cells for confocal microscopy analysis were performed as we previously described (23). Mitotracker and Topro (Molecular Probes) were used as markers for mitochondria and nuclei, respectively. The antihemagglutinin (anti-HA) tag Ab (Cell Signaling) was used for detection of the HA-tagged MCJ, followed by the anti-rabbit secondary Ab (Molecular Probes). Samples were examined by confocal microscopy using a Zeiss LSM 510 Meta confocal laser scanning imaging system (Carl Zeiss Microimaging).

Immunoelectron microscopy analysis. Immunoelectron microscopy analysis for MCJ was performed as we previously described (23) using fixed embedded preparations of MCJ-transfected 293T cells, freshly isolated CD8 T cells, or heart tissue. The anti-mouse MCJ rabbit polyclonal Ab was used for detection of MCJ. For electron microscopy of supercomplexes, the gel eluate was directly applied to continuous carbon-coated grids and deep stain embedded in ammonium molybdate (30).

Histology and serum biochemistry analysis. For histological analysis, livers and kidneys were harvested, fixed in formalin, and paraffin embedded. Tissue sections from paraffin-embedded blocks were stained with H&E according to routine procedures. Images were obtained with the $EVOS_{XL}$ Core microscope (AMG). For analysis of lipid accumulation in the liver, freshly harvested livers were frozen in OCT, and frozen sections were stained for Oil Red O. For histological analysis of glycogen, periodic acid-Schiff (PAS) staining was performed in paraffin-embedded liver and kidney sections. The levels of glycogen in liver extracts (corresponding to 1 mg) were determined using the Glucose (HK) Assay kit, as recommended by the manufacturer (Sigma). Levels of triglycerides in sera were determined using the triglyceride colorimetric kit and ketone body kit (Cayman Chemicals), as recommended by the manufacturer. The levels of free fatty acids (FFA) in serum and liver extracts were determined using the free fatty acid quantification kit (Biovision) as recommended by the manufacturer. The levels of cholesterol in the liver extracts (corresponding to 1 mg) were determined using the Abcam kit. Glucose levels in blood were determined using the glucose-monitoring system (LifeScan).

Complex I activity. Analysis of complex I activity was performed using mitochondrial extracts generated following the protocol for the purification of complex I. Activity was measured using the complex I enzyme activity microplate assay kit (MitoSciences) as recommended by the manufacturer. Assays were performed using a total of 1 μg (heart) or 1.8 μg (T cells) of mitochondrial extracts or 5 to 10 μl of supercomplex eluates.

Intracellular ATP level determination. The levels of intracellular ATP in 10^4 MCF7 cells or 10 μg of protein from liver extracts were determined using the ATPlite luminescence ATP detection assay system (PerkinElmer) by following the recommendations from the manufacturer and a TD-20/20 luminometer (Turner Biosystems).

RESULTS

Identification of murine MCJ/DnaJC15 reveals a conserved tissue expression pattern with the human ortholog. MCJ/DnaJC15 expression has been examined in human ovarian and breast cancer cells (16, 17, 20, 23). We have previously reported that MCJ originated in vertebrates, where it is highly conserved (23), but no studies have reported its murine counterpart. Comparative analysis of human and mouse MCJ protein sequences showed an overall 75% identity (Fig. 1A), with nearly identical transmembrane and C-terminal DnaJ domain regions, as well as a highly conserved (57%) N-terminal region (1 to 35 amino acids). To identify the tissue expression pattern of the murine MCJ gene, we performed Northern blot analysis. MCJ mRNA was highly abundant in the heart, followed by liver and kidney (Fig. 1B). Although MCJ is expressed in some human cancer cells, the specific distribution of MCJ expression in normal human tissues remains unknown. Northern blot analysis of nonmalignant human tissues showed a distribution of human *mcj* gene expression similar to that of the murine *mcj* gene (Fig. 1C). Previous microarray analyses performed using CD8 T cells indicated that MCJ was also present in this immune cell type (data not shown). To further investigate the expression of MCJ in the different populations of the immune system, isolated CD4 and CD8 T cells, as well as B cells from mouse spleen and lymph nodes, were used to perform real-time RT-PCR for *mcj* expression. Interestingly, *mcj* gene expression was very high in CD8 T cells but almost undetectable in CD4 T cells and B cells (Fig. 1D).

We generated an Ab that specifically recognizes the N-terminal region of mouse MCJ, as confirmed by Western blotting of 293T cells transfected with murine MCJ (Fig. 1E). The expression of endogenous MCJ protein in mouse tissues was examined by Western blotting using this Ab. Consistent with the mRNA expression analysis, MCJ protein was present in heart, liver, and kidney but almost undetectable in lungs (Fig. 1F). MCJ protein also was abundant in CD8 T cells but low in CD4 T cells (Fig. 1G). Thus, MCJ/DnaJC15 has a restricted tissue and cellular distribution.

MCJ/DnaJC15 is a novel mitochondrial-resident cochaperone. To dissect the potential function of MCJ in normal tissue, we examined the localization of endogenous MCJ in the heart under physiological conditions by immunoelectron microscopy (IEM). Most MCJ immunoreactivity was found in clearly defined mitochondria, predominantly at the inner membrane (Fig. 2A). In purified CD8 T cells, IEM analysis also showed that MCJ localizes almost exclusively at the mitochondria (Fig. 2B). To further demonstrate the mitochondrial localization of endogenous MCJ, we performed Western blot analysis of MCJ in murine heart mitochondrial and cytosolic fractions. High levels of MCJ were found in the mitochondrial fraction, while it was almost undetectable in the cytosolic fraction (Fig. 2C). The purity of the fractions was determined by the expression of complex IV (subunit CoxIV) of the respiratory chain as a marker of mitochondria and GAPDH as a marker of the cytosolic fraction (Fig. 2C). In addition, analysis of

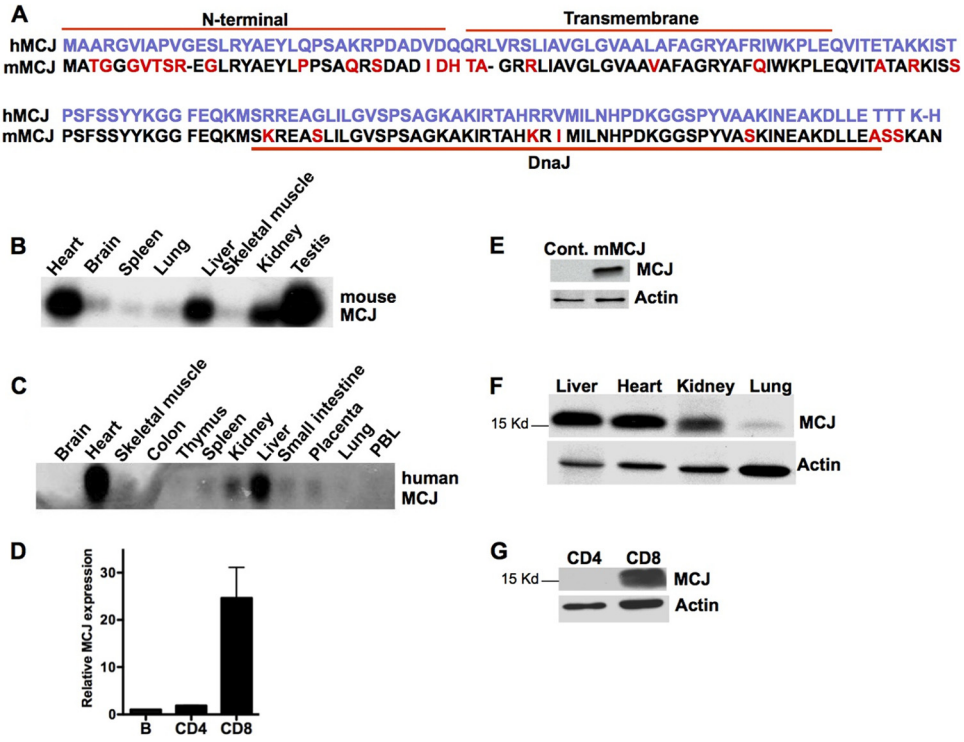

FIG 1 Specific tissue distribution of mouse and human MCJ/DnaJC15. (A) Alignment of protein sequences of human MCJ/DnaJC15 (hMCJ) and its ortholog in the mouse (mMCJ) and differences in amino acids (red). (B) Northern blot analysis of mouse normal tissue poly(A) mRNA using a specific mouse *mcj* probe. (C) Northern blot analysis of human normal tissue poly(A) mRNA using a specific human *mcj* probe. (D) Real-time RT-PCR for *mcj* using RNA from mouse B cells, CD4 T cells, and CD8 T cells. mRNA levels were normalized to β_2 microglobulin. The error bars indicate standard deviations. (E) Whole-cell extracts from 293T cells transfected with a mouse *mcj*-expressing plasmid (mMCJ) or an empty plasmid (Cont.) were examined for mouse MCJ expression (MCJ) by Western blotting. Actin was examined as a loading control. (F) Endogenous MCJ protein expression in mouse liver, heart, kidney, and lung was examined by Western blotting. Actin expression was examined as a loading control. (G) Endogenous MCJ protein expression in mouse CD4 T cells and CD8 T cells was examined by Western blotting.

calreticulin (an endoplasmic reticulum marker) and syntaxin 11 (a marker for the Golgi/endosome compartment) showed no significant contamination of these fractions within the mitochondrial fraction (Fig. 2D). Similar to the localization in the heart, MCJ was also almost exclusively present in the mitochondrial fraction of purified mouse CD8 T cells (Fig. 2E). Furthermore, Western blot analysis of endogenous human MCJ in the breast cancer MCF7 cell line also showed the presence of MCJ primarily in mitochondria (Fig. 2F).

Since the immune staining obtained by electron microscopy (EM) suggested that MCJ localized in the inner membrane, to verify the sublocalization within mitochondria, we isolated the inner membrane mitochondrial fraction and performed Western blot analysis. An abundance of MCJ was present in the inner membrane fraction relative to whole mitochondrial extracts (Fig. 2G). A similar distribution was observed for CoxIV, the subunit of complex IV known to be embedded in the inner membrane of the mitochondria (Fig. 2G). In contrast, residual amounts of Bcl-x_L, a mitochondrial outer membrane protein, were detected in the inner membrane fraction (Fig. 2G). Thus, endogenous MCJ localizes in mitochondria, and within the mitochondria it is targeted to the inner membrane.

MCJ functions as a negative regulator of mitochondrial membrane potential and ATP production. A major function of mitochondria is to provide ATP as a source of energy for the cell through oxidative phosphorylation. To determine whether MCJ could modulate mitochondrial function, we compared ATP levels in MCF7 breast cancer cells that express MCJ (23) with the levels in the MCF7/siMCJ cell line derived from MCF7 cells where MCJ expression was knocked down by an MCJ short hairpin RNA (shRNA) (23). Surprisingly, the levels of ATP in MCF7/siMCJ cells were markedly higher than in MCF7 cells (Fig. 3A). To show that the elevated levels of ATP were derived from mitochondria, MCF7/siMCJ cells were treated with rotenone, an inhibitor of complex I in the ETC, for a short time (7 h). Rotenone did not affect the viability of MCF7/siMCJ cells during this period of treatment (Fig. 3B). However, it caused a drastic reduction in the levels of ATP in these cells (Fig. 3C). Thus, MCJ negatively regulates mitochondrial ATP production, and loss of MCJ leads to increased levels of ATP.

The generation of ATP by the ATP synthase (complex V) in mitochondria is dependent on the presence of an MMP, generated by the accumulation of H^+ provided by the ETC complexes I, III, and IV. Since MCJ localized at the inner membrane of the mitochondria, we argued that it could act as a negative regulator of the proton gradient. To address this possibility, we compared MMP in the two types of T cells that express very different levels of MCJ, with CD8 T cells expressing high levels of MCJ relative to CD4 T cells. Interestingly, mitochondria were depolarized in most CD8 T cells compared with CD4 T cells, correlating with the selective presence of MCJ in CD8 T cells (Fig. 3D). The ETC can also contribute to the generation of mitochondrial reactive oxygen species

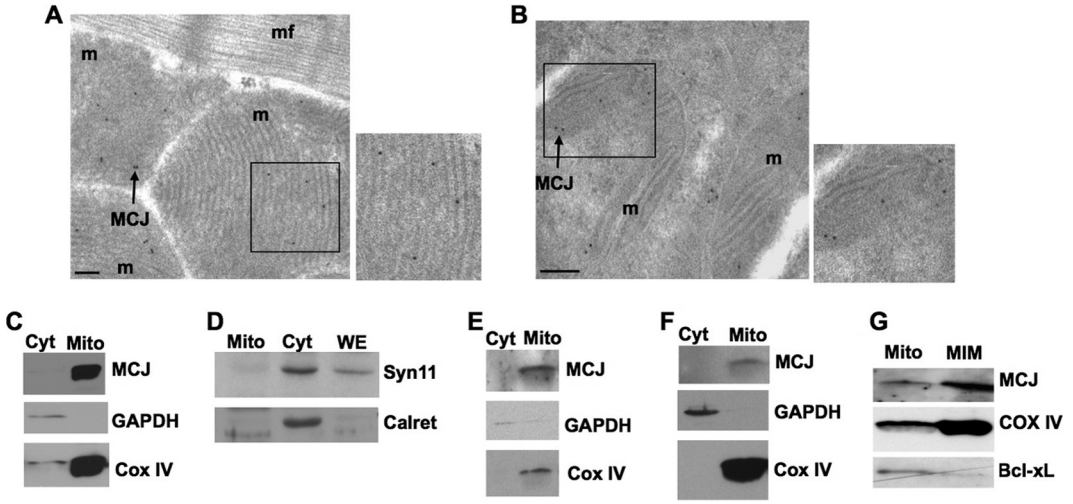

FIG 2 Endogenous MCJ localizes to the mitochondria. (A and B) Immunoelectron microscopy analysis of endogenous MCJ in heart (A) and purified CD8 T cells (B) from wild-type mice. Electron-dense gold particles represent MCJ (the arrows point to representative immunoreactivities). Higher magnifications of the boxed areas are shown on the right. m, mitochondria; mf, myofibrils. Magnification, ×20,000. Bars, 200 nm. (C) MCJ expression in purified cytosolic (Cyt) and mitochondrial (Mito) extracts from mouse heart by Western blotting. GAPDH was used as a marker for the cytosolic fraction, and CoxIV was used as a marker for the mitochondrial fraction. (D) Syntaxin 11 (Syn11) and calreticulin (Calret) expression in purified cytosolic and mitochondrial extracts, as well as whole-cell extracts (WE) from mouse heart. (E and F) MCJ expression in purified cytosolic and mitochondrial extracts from mouse CD8 T cells (E) and human MCF7 cells (F) was examined by Western blotting. (G) MCJ expression in purified whole mitochondrial extracts (Mito) and mitochondrial inner membrane fraction extracts (MIM) from mouse heart. CoxIV and Bcl-x_L were used as markers for the mitochondrial inner and outer membrane, respectively.

(mROS) due to electron escape (31). Unlike MMP, analysis of mROS by staining with MitoSox-Red and flow cytometry showed no difference in the levels of mROS between CD4 and CD8 T cells (Fig. 3E). Thus, it was possible that the selective differences in mitochondrial membrane potential could be specifically mediated by the presence of MCJ.

To demonstrate the negative role of MCJ in mitochondrial membrane potential and function, we generated MCJ-deficient mice. The genotype of MCJ-deficient mice was confirmed by Southern blotting (Fig. 3F). To confirm the loss of MCJ protein expression, we examined endogenous MCJ protein levels in different tissues by Western blotting. MCJ was detected in heart, liver, and CD8 cells from wild-type mice but not in MCJ KO mice (Fig. 3G). In addition, no MCJ mRNA could be detected in the MCJ-targeted mice, confirming the loss of MCJ expression (Fig. 3H). MCJ mRNA levels were also reduced in the heterozygous mice compared to wild-type mice (Fig. 3H), suggesting that MCJ expression may be dependent on the allele copy number. Disruption of MCJ expression did not affect the viability of the mice up to the examined age (approximately 1 year). Both male and female MCJ-deficient mice were fertile and did not exhibit any obvious malformations or behavioral abnormalities (data not shown). Thus, MCJ is not essential for development and/or organ function under normal physiological conditions.

We then examined MMP in CD8 T cells isolated from wild-type and MCJ KO mice to determine whether MCJ contributes to maintaining mitochondria in a depolarized state in these cells. Mitochondria in most CD8 cells deficient in MCJ were hyperpolarized compared with mitochondria from wild-type cells (Fig. 3I). Increased MMP in the MCJ-deficient CD8 cells did not result in increased production of mROS (Fig. 3J), suggesting that loss of MCJ facilitates ETC activity, leading to increased accumulation of H^+ in the intermembrane space while minimizing electron escape from the ETC. MCJ deficiency did not affect the MMP (Fig. 3K) or mROS (Fig. 3L) in CD4 T cells, consistent with the low level of MCJ present in these cells.

Together, the results demonstrate that MCJ is a negative regulator of the mitochondrial respiratory chain and that it prevents the mitochondrial hyperpolarization state and restricts mitochondrial generation of ATP.

MCJ associates with and inhibits complex I in the mitochondrial electron transfer chain. To investigate the molecular mechanism by which MCJ could regulate the mitochondrial membrane potential and find potential partners at the ETC, we performed a phage display screening using the N-terminal region of MCJ as bait. The results from the screening revealed one of the subunits of complex I (NDUFv1) within the mitochondrial ETC as a potential interacting protein with MCJ (data not shown). To determine whether MCJ associates with complex I, we performed coimmunoprecipitation analysis using heart mitochondrial extracts generated by lauryl-maltoside, a detergent that solubilizes complexes from the membrane but preserves the structure of the multisubunit complex I as a monomer. Complex I was immunoprecipitated from mitochondrial extracts, and the presence of MCJ in the immunoprecipitates was examined by Western blotting. MCJ was present in the complex I immunoprecipitate from wild-type but not MCJ KO mice (Fig. 4A). As a control for the immunoprecipitation, we examined the expression of NDUFA9 and NDUFS3, two well-characterized subunits of complex I (Fig. 4A). Neither CoxIV (a complex IV subunit) nor cytochrome *c* could be detected in complex I immunoprecipitates (Fig. 4B), further showing the specificity of the complex I immunoprecipitation. We also examined whether MCJ interacted with other complexes of the respiratory chain. No MCJ could be found in immunoprecipitates for complex III (Fig. 4C). Thus, MCJ preferentially associated with complex I of the mitochondrial ETC.

To determine whether MCJ could be a regulator of complex I, we examined complex I activity in maltoside-solubilized mito-

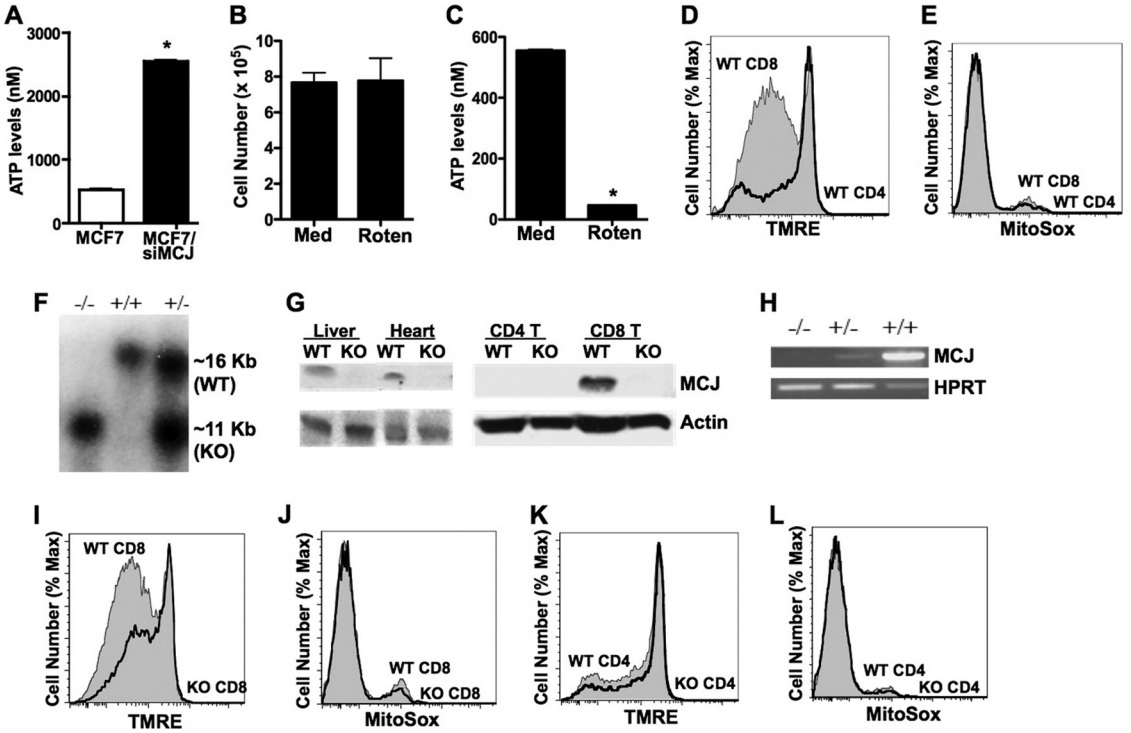

FIG 3 MCJ depolarizes mitochondria and decreases ATP levels. (A) Intracellular ATP levels in MCF7 cells and MCF7/siMCJ cells (10^4 cells) incubated in medium. The error bars indicate standard deviations. (B) Cell recovery of MCF7/siMCJ cell cultures after incubation in medium alone (Med) or rotenone (Roten) (10 μM) for 7 h; 5×10^5 cells were plated the day before the treatment. (C) Intracellular ATP levels in MCF7/siMCJ cells (10^4 cells) after incubation in medium or rotenone for 7 h. (D) MMP in freshly isolated wild-type (WT) CD8 T cells and WT CD4 T cells was determined by staining with TMRE and flow cytometry analysis. (E) mROS in freshly isolated WT CD8 T cells and WT CD4 T cells was determined by staining with MitoSox-Red and flow cytometry analysis. (F) Southern blot analysis showing MCJ-targeted (~11-kb) and wild-type (~16-kb) alleles in wild-type (+/+), heterozygous (+/−), and MCJ KO (−/−) mice. (G) Western blot analysis for MCJ in whole-cell extracts from liver, heart, and CD4 and CD8 T cells from WT and MCJ KO mice. Actin was analyzed as a loading control. (H) RT-PCR for MCJ using RNA from CD8 T cells isolated from WT, MCJ KO, and MCJ heterozygous mice. HPRT expression was examined as a control. (I) MMP in freshly isolated WT CD8 T cells and MCJ KO CD8 T cells was determined as in panel D. (J) mROS in freshly isolated WT CD8 T cells and MCJ KO CD8 T cells was determined as in panel F. (K) MMP in freshly isolated WT CD4 T cells and MCJ KO CD4 T cells. (L) mROS in freshly isolated WT CD4 T cells and MCJ KO CD4 T cells. *, $P < 0.05$. Statistical significance was determined by Student's *t* test. The data are representative of three independent experiments.

chondrial extracts obtained from the hearts of wild-type and MCJ KO mice. Interestingly, higher complex I activity was detected in MCJ-deficient hearts than in wild-type hearts (Fig. 4D). The levels of complex I in mitochondria, however, were comparable between wild-type and MCJ-deficient hearts, as determined by Western blotting for NDUFA9 (Fig. 4E). To further confirm that MCJ acts as a negative regulator of complex I, we examined complex I activity in freshly isolated wild-type and MCJ KO CD8 T cells, as well as wild-type CD4 T cells. The levels of NDUFA9 and NDUFS3 in the mitochondrial extracts were comparable among the three cell types (Fig. 4F). In contrast, complex I activity was markedly lower in wild-type CD8 T cells than in wild-type CD4 T cells, correlating with the presence of MCJ in CD8 T cells (Fig. 4G). More importantly, complex I activity was increased in MCJ KO CD8 T cells compared with the activity in wild-type CD8 T cells and was comparable to that in wild-type CD4 T cells (Fig. 4G). Together, these results show that MCJ is an endogenous negative regulator of complex I of the respiratory chain in mitochondria.

Loss of MCJ facilitates the formation of active respiratory chain supercomplexes. Several studies in bacteria and eukaryotic systems (including mammals) have shown that complexes of the mitochondrial ETC associate to form supercomplexes to facilitate the transfer of electrons between complexes (32). The formation of these supercomplexes seems to be a dynamic process. To further show the physical interaction of MCJ with complex I and to investigate its presence in supercomplexes, we performed BN gel electrophoresis using mitochondrial extracts generated with digitonin, a mild detergent that preserves the supercomplexes (5). Complexes from the first-dimension BN electrophoresis (Fig. 5A) were resolved by denaturing second-dimension electrophoresis (2D BN/SDS-PAGE), followed by Western blotting for MCJ. The blots were further reprobed for subunits of the specific complex to localize each of the complexes. The pattern obtained for NDUFA9 (complex I), Core1 (complex III), and CoxIV (complex IV) correlated with the previously described patterns in bovine heart (29). The most prominent band for MCJ colocalized with monomeric complex I (Fig. 5B). A weaker signal for MCJ could also be detected at the dimeric complex III (Fig. 5B). These results further demonstrate that MCJ preferentially interacts with complex I, although it may also have some weak interaction with complex III that cannot be maintained when mitochondria are solubilized with maltoside (Fig. 4C), in contrast to its interaction with complex I.

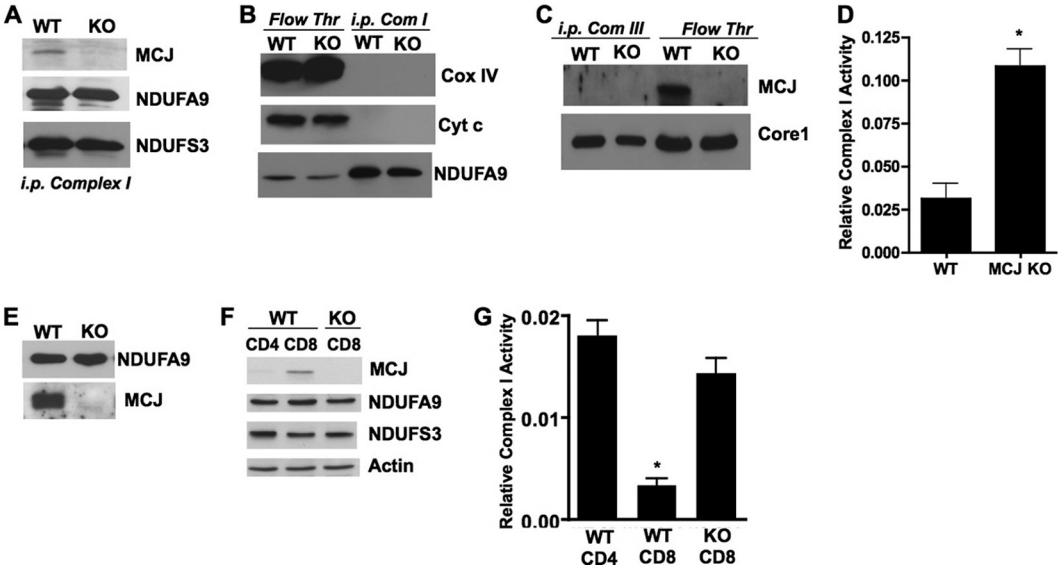

FIG 4 MCJ is a repressor of mitochondrial respiratory chain complex I activity. (A) The presence of MCJ, NDUFA9, and NDUFS3 in immunoprecipitates of complex I from mitochondrial extracts generated from WT and MCJ KO hearts was examined by Western blotting. (B) The presence of CoxIV, cytochrome *c* (Cyt c), and NDUFA9 in immunoprecipitates of complex I (i.p. Com I) and in the flowthrough extracts resulting from the immunoprecipitation (Flow Thr) using extracts from WT and MCJ KO hearts was examined by Western blotting. (C) The presence of MCJ and Core1 protein of complex III in immunoprecipitates of complex III (i.p. Com III) and flowthrough using mitochondrial extracts from WT and MCJ KO hearts was examined by Western blotting. (D) Relative complex I activities in mitochondrial extracts (10 μg) from WT and MCJ KO mouse hearts. The error bars indicate standard deviations. (E) Expression of NDUFA9 and MCJ in heart mitochondrial extracts from WT and MCJ KO mice was examined by Western blotting. (F) Expression of MCJ, NDUFA9, NDUFS3, and actin in mitochondrial extracts from WT CD4, WT CD8, and MCJ KO CD8 T cells was examined by Western blotting. (G) Relative complex I activity in mitochondrial extracts (5 μg) from freshly isolated WT CD4, WT CD8, and MCJ KO CD8 T cells. *, $P < 0.05$. Statistical significance was determined by the Student *t* test.

Since MCJ associated preferentially with monomeric complex I rather than supercomplexes containing complex I, we decided to examine whether MCJ could affect the formation of these supercomplexes, considering that complex I seems to initiate the assembly of the supercomplexes (5, 8, 32). Digitonin-solubilized mitochondrial extracts from wild-type and MCJ KO hearts were resolved by a single-dimension BN electrophoresis. While no differences could be observed regarding the presence of individual complexes, an abundance of supercomplexes appeared to be present in mitochondria from MCJ KO mice (Fig. 5C). Magnification of the supercomplex region of the BN showed the presence of previously defined supercomplex bands (5, 6, 29) in MCJ KO mice (Fig. 5C). The selective accumulation of supercomplexes in mitochondria of MCJ KO mice was reproducible among independent preparations of mitochondria from different sets of mice (Fig. 5D). Unlike digitonin, maltoside disrupts supercomplexes primarily by affecting the association of complex I with the other complexes, although it does not seem to affect complex III/IV dimers (5). As expected, no supercomplexes were detected in BN electrophoresis of maltoside-generated mitochondrial extracts in either wild-type or MCJ KO mice (Fig. 5E). In addition, no obvious difference in the pattern of bands was observed between wild-type and MCJ KO mice (Fig. 5E), supporting the idea that MCJ deficiency has a selective effect on the formation of supercomplexes.

To further show the accumulation of supercomplexes in the absence of MCJ, we performed BN-PAGE with digitonin-solubilized mitochondrial extracts, followed by Western blotting of the BN gel for specific ETC complex subunits. Mitochondrial extracts from MCJ KO mice contained higher levels of NDUFA9 (complex I) in the supercomplex region than wild-type mitochondrial extracts (Fig. 5F, sc). The levels of CoxIV (complex IV) and Core1 (complex III) in the supercomplex region in MCJ KO mice were also increased compared with the levels in wild-type mice (Fig. 5F, sc). The levels of monomeric complex I, complex III dimer, and monomeric complex IV were comparable between wild-type and MCJ-deficient mice (Fig. 5F). Thus, MCJ deficiency facilitates the formation of the supercomplexes.

To determine whether the supercomplexes in mitochondria from MCJ KO mice contained active complex I, we performed in-gel NADH dehydrogenase activity assays using BN-PAGE. NADH dehydrogenase (purple) was detected in monomeric complex I in both wild-type and MCJ KO mitochondria (Fig. 6A). However, there was an accumulation of NADH dehydrogenase activity in the supercomplex area in MCJ KO mice (Fig. 6A). Magnification of the region showed the presence of active supercomplexes (Fig. 6A, right). To further show the increased supercomplex activity in the absence of MCJ, we performed BN-PAGE, followed by excision of the supercomplex region of the BN gel, elution of the proteins from the excised gel, and measurement of complex I activity in the eluates. We first corroborated by SDS-PAGE the presence of complex I in the supercomplex eluates. According to the increased levels of supercomplexes in MCJ KO mice, increased levels of NDUFA9 were present in the BN gel eluates in MCJ KO mice (Fig. 6B). Furthermore, we corroborated the presence of supercomplexes after gel elution by electron microscopy of the eluates. Supercomplexes were clearly visible (Fig. 6C) and were confirmed by comparison with projections of previously published three-dimensional (3D) structure (30). Analysis of complex I activity in the eluted super-

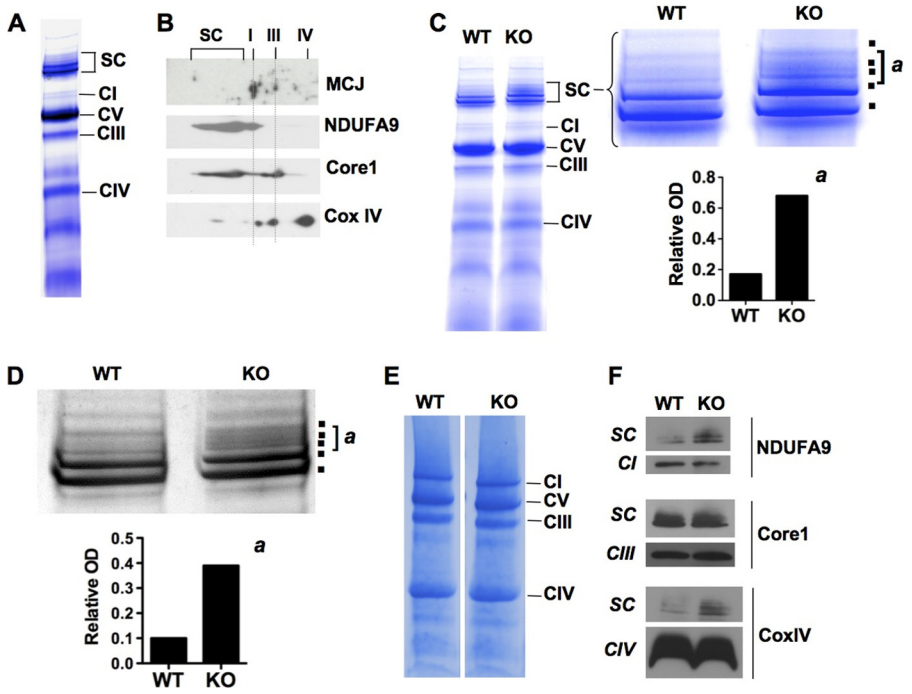

FIG 5 Loss of MCJ facilitates the formation of ETC supercomplexes. (A) BN gel electrophoresis of digitonin-solubilized mitochondrial extracts from wild-type heart. Monomeric complex I (CI), dimer complex III, monomeric complexes IV and V, and supercomplexes (SC) are marked. (B) Digitonin-solubilized mitochondrial extracts from mouse heart were resolved in 2D-BN/SDS-PAGE. Western blot analysis for MCJ, NDUFA9, complex III Core1 protein, and CoxIV was performed. (C) BN electrophoresis of digitonin-solubilized mitochondrial extracts from WT and MCJ KO mouse hearts. (Right) Magnification of the supercomplex (SC) area. Squares denote individual supercomplex bands. Below (a) is shown the densitometry of the supercomplex "a" area. OD, optical density. (D) Magnification of the supercomplex region from a different BN gel with mitochondrial extracts (digitonin) from an independent set of WT and MCJ KO mouse hearts. Below (a) is shown the densitometry of the supercomplex "a" area. (E) BN-PAGE of maltoside-solubilized mitochondrial extracts from WT and MCJ KO hearts. Monomeric complex I, dimer complex III, and monomeric complexes IV and V are marked. (F) BN-PAGE of digitonin-solubilized mitochondrial extracts from WT and MCJ KO hearts transferred into a membrane (Western blot) and immunoblotted for NDUFA9, CoxIV, and Core1 protein. Immunoreactivity for the three proteins within the supercomplex (SC) region is shown. Immunoreactivity for NDUFA9 with monomeric complex I (CI), Core1 with dimeric complex III (CIII), and CoxIV with monomeric complex IV (CIV) is shown.

complexes from three independent sets of mice consistently showed increased activity in MCJ KO mice (Fig. 6D). Thus, MCJ interferes with supercomplex formation in the ETC, and the loss of MCJ causes an accumulation of active supercomplexes in mitochondria.

Loss of MCJ prevents lipid accumulation and steatosis in the liver in response to metabolic changes. The role of MCJ as a negative regulator of complex I in mitochondria suggested that MCJ could play a major role in decreasing mitochondrial respiration under altered metabolic conditions. Fasting causes drastic metabolic changes by triggering the hydrolysis of triglycerides stored in the adipose tissue to FFA that are then mobilized and transported to the liver, where they undergo mitochondrial β-oxidation. We therefore examined whether increased mitochondrial respiration in the absence of MCJ affected lipid metabolism in the liver. Histological analysis of the liver under normal (feeding) conditions showed no detectable difference between wild-type and MCJ-deficient mice (Fig. 7A). The livers of wild-type mice fasted for 36 h showed clear signs of steatosis, as determined by the presence of hepatocytes with large cytoplasm (Fig. 7A). In contrast, livers from fasted MCJ KO mice did not display signs of steatosis (Fig. 7A). Analysis of lipids in frozen sections of liver from fasted wild-type mice by Oil Red O staining showed the accumulation of large amounts of lipids, as expected (Fig. 7B). However, marginal lipid accumulation in livers from fasted MCJ KO mice could be detected (Fig. 7B). The expression levels of carnitine palmitotransferase and peroxisome proliferator-activated receptor α genes, induced in response to fasting, were comparable in fasted MCJ KO and wild-type mice (data not shown), indicating that MCJ KO mice were undergoing a fasting response. These results suggested that a sustained mitochondrial oxidation of FFA in MCJ KO mice leads to rapid metabolism of lipids and minimizes their accumulation in the liver. Accordingly, we also observed a more prominent loss of white fat in MCJ KO mice after fasting than in wild-type mice (data not shown). We therefore decided to examine the serum triglyceride and FFA levels after fasting and found lower levels of both triglycerides (Fig. 7C) and FFA (Fig. 7D) in MCJ KO mice than in wild-type mice. Although enhanced β-oxidation of FFA during starvation is associated with increased production of ketone bodies by the liver, the serum levels of ketone bodies were similar in wild-type and MCJ KO mice after fasting (Fig. 7E). The levels of triglycerides (Fig. 7E), FFA (Fig. 7F), and ketone bodies (Fig. 7H) in normally fed mice were lower than in fasted mice but comparable between wild-type and MCJ KO mice. Thus, under physiological conditions (normal diet), MCJ appears to be dispensable, but in response to fasting, the loss of MCJ facilitates lipid metabolism in the liver, consistent with its negative effect on mitochondrial function.

Interestingly, despite accelerated metabolism during fasting, weight loss caused by the fasting in MCJ KO mice was not statis-

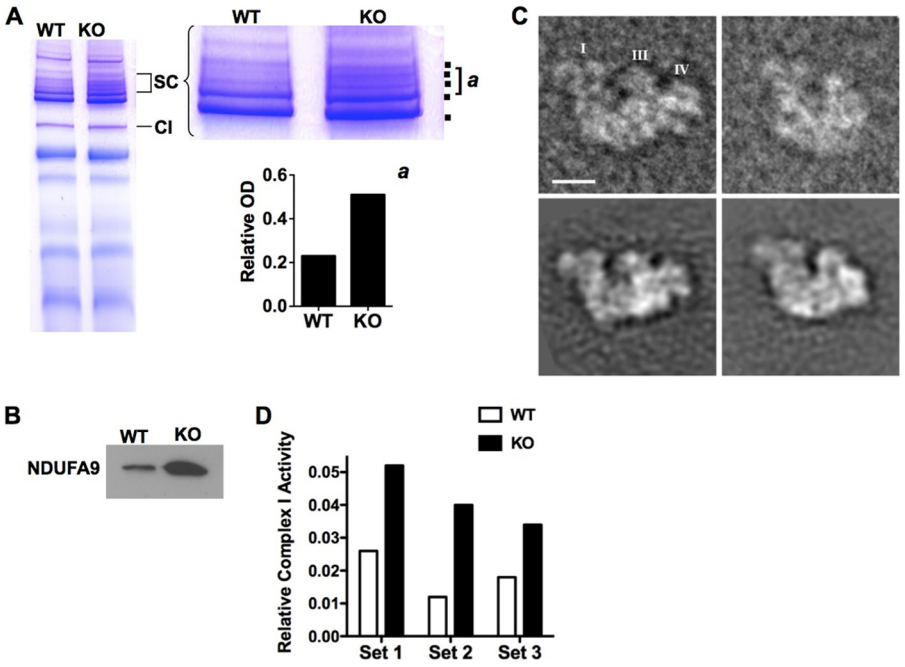

FIG 6 MCJ is a negative regulator of complex I activity in supercomplexes. (A) In-gel NADH dehydrogenase activity in BN electrophoresis using digitonin-mitochondrial extracts from WT and MCJ KO mouse hearts. The purple bands represent those containing NADH dehydrogenase activity (complex I and supercomplexes). On the right is shown a magnification of the supercomplex area. Squares denote individual supercomplex bands. Below (a) is shown the densitometry of the supercomplex "a" area. (B) Western blot analysis for NDUFA9 in eluates from the supercomplex regions of BN gels using digitonin-solubilized mitochondrial extracts from WT and MCJ KO hearts. (C) (Top) Images from electron micrographs of MCJ-KO supercomplexes eluted from a blue native gel. Complexes I, III, and IV are indicated. Scale bar, 100 Å. (Bottom) Two projections calculated from the 3D structure of the bovine supercomplex (EMDataBank entry EMD-5319). (D) Relative complex I activities in eluates of supercomplex regions of BN gels using digitonin-solubilized mitochondrial extracts from WT and MCJ KO hearts. Each set represents independent mitochondrial preparations from individual mouse hearts (total, 3 WT and 3 KO mice) and independent BN-PAGE/elutions.

tically different from the weight loss in wild-type mice (Fig. 8A); even the initial weights were comparable in the two groups (Fig. 8B). In addition, the analysis of glucose levels in blood during fasting showed no statistically significant differences between MCJ KO and wild-type mice, either during the initial drop in glucose (12 h) (Fig. 8C) or the recovery (Fig. 8D). These results suggested the presence of mechanisms to balance the accelerated lipid metabolism in the liver in the absence of MCJ. Increased β-oxidation of FFA in the liver by mitochondria could lead to increased levels of ATP (through β-oxidation), as well as glycerol, resulting from the lipid breakdown. The accumulation of ATP and glycerol can be sensed by the liver as a signal to initiate glycogenesis (an energy-costly process) to store the excess energy. Analysis of ATP levels in the liver after fasting confirmed increased ATP levels in the livers of MCJ KO mice relative to the livers of wild-type mice (Fig. 8E). We therefore examined glycogen levels in the liver by PAS staining. Glycogen was almost undetectable in the livers of fasted wild-type mice, as expected (Fig. 8F). However, high levels of glycogen accumulated in the livers of fasted MCJ KO mice (Fig. 8F). In addition to the liver, glycogenesis can occur to a lesser extent in the cortex of kidneys. Accumulation of glycogen could also be found in some areas of the kidneys in fasted MCJ KO mice by PAS staining (data not shown). Biochemical analysis of glycogen in liver extracts further demonstrated the selective accumulation of glycogen in fasted MCJ KO mice (Fig. 8G). No difference could be found between the basal levels of glycogen in the liver in nonfasted wild-type mice and nonfasted MCJ KO mice (Fig. 8G). The accumulation of glycogen instead of lipids in the livers of fasted MCJ KO mice correlated with an increased ratio of liver to body weight relative to wild-type mice (Fig. 8H). Glycogen is synthesized by glycogen synthase using UDP-glucose as the substrate. Glycogen synthase levels were upregulated in livers from fasted MCJ KO mice relative to wild-type mice (Fig. 8I). In contrast, the levels of PEPCK, an essential gluconeogenic enzyme in the synthesis of glucose from pyruvate, were comparable in fasted WT and MCJ KO mice (Fig. 8I), suggesting that the glycogen present in the livers of MCJ KO mice was likely generated with glucose resulting from triglyceride hydrolysis.

According to its negative role in mitochondrial respiration, these results show that MCJ is an essential regulator of liver metabolism during fasting and that the absence of MCJ favors lipid degradation and glycogenesis in the liver. To address whether MCJ could also play a role in regulating metabolism in response to other altered dietary conditions, we investigated its effect in response to a high-cholesterol diet, since this is currently a major health problem worldwide. Wild-type and MCJ KO mice were fed a high-cholesterol diet for 4 weeks (24, 33). High levels of cholesterol accumulated in the livers of wild-type mice fed the high-cholesterol diet (Fig. 8J). In contrast, significantly lower cholesterol levels were detected in MCJ KO mice fed the same diet (Fig. 8J). Similar low levels of cholesterol were present in livers from wild-type and MCJ KO mice fed a normal diet (Fig. 8K). Thus, MCJ may modulate the effects caused by a variety of metabolic disorders.

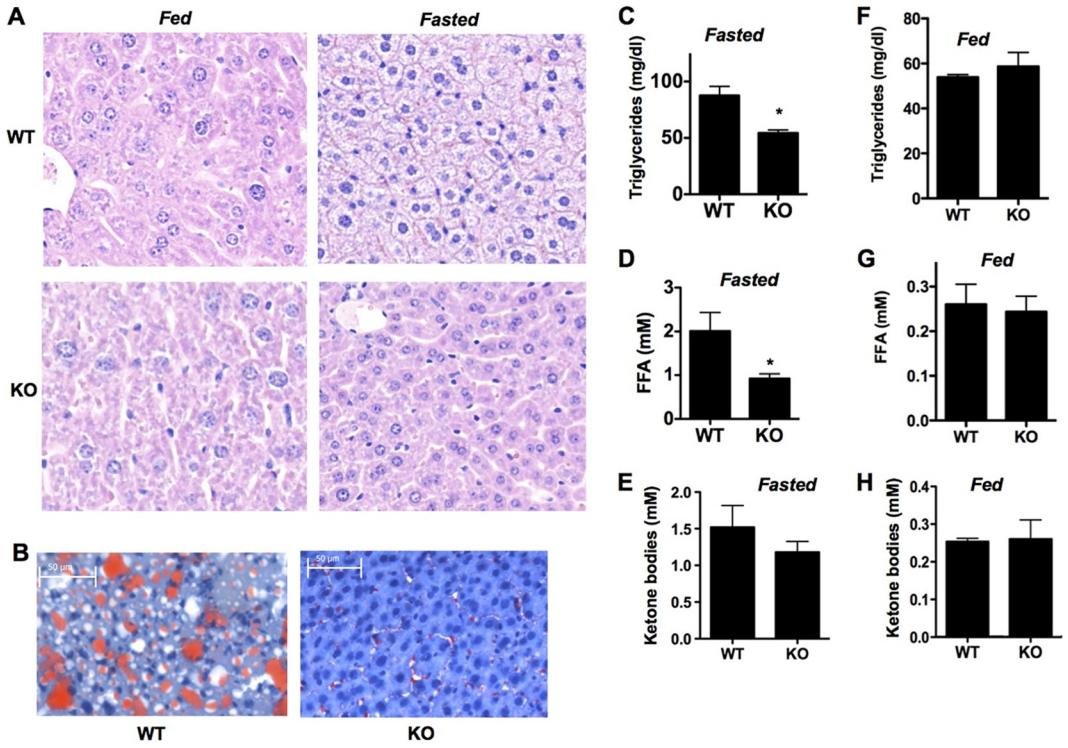

FIG 7 MCJ deficiency enhances liver lipid metabolism during fasting. (A) Liver histology by H&E staining from WT and MCJ KO mice under normal or fasted conditions. Magnification, ×200. (B) Sections from frozen livers of fasted wild-type and MCJ KO mice were stained with Oil Red O for detection of lipids. (C to E) Serum triglyceride levels (C), FFA (D), and ketone bodies (E) in fasted WT and MCJ KO mice ($n = 4$). (F to H) Serum triglyceride levels (F), FFA (G), and ketone bodies (H) in normally fed WT and MCJ KO mice ($n = 3$). *, $P < 0.05$. Statistical significance was determined by Student's t test. The error bars indicate standard deviations.

DISCUSSION

The DnaJ family is the largest of the cochaperone families, but the functions of most mammalian DnaJ members in primary tissues remain to be elucidated. In this study, we describe for the first time the murine ortholog for human MCJ (DnaJC15) and the conserved expression pattern that this cochaperone has between the two species. Using imaging and biochemical approaches, we show that MCJ localizes in mitochondria in primary cells, and within mitochondria, it is targeted to the inner membrane. Based on overexpression studies of MCJ, we previously reported that MCJ was not localized in mitochondria (23). This apparent discrepancy is explained by a rapid depolarization of mitochondria and mitochondrial swelling caused by the overexpression of MCJ (data not shown), correlating with the negative role of MCJ on complex I and MMP described in this study. Proteomics studies performed to characterize the mitochondrial proteome also identified MCJ as a protein localized in mitochondria (34). In addition, a recent study has also reported the presence of human MCJ in the mitochondrial inner membrane (35). Interestingly, while most proteins present in mitochondria are required to maintain mitochondrial functions, here we identify MCJ as a negative regulator. Loss of MCJ leads to increased mitochondrial membrane potential and, consequently, increased ATP production. Furthermore, we show that one of the mechanisms by which MCJ maintains lower mitochondrial respiration is through its negative regulation of complex I. Thus, in the absence of MCJ, there is a significant increase in complex I activity. While a number of associated proteins have been shown to be required for complex I to be fully active (36), to our knowledge, MCJ is one of the few molecules that repress its activity. Intriguingly, a significant change in complex I during evolution was the acquisition of both nonactive and active forms in vertebrates, while only the active form has been identified in prokaryotes (37, 38). Thus, mammalian complex I is a mixture of both active and nonactive forms. The mechanisms that regulate the balance between the forms remain unclear. Since MCJ originated in vertebrates and represses complex I activity, we speculate that MCJ regulates the balance between complex I active and nonactive forms. However, we also show here that loss of MCJ results in accumulation of supercomplexes in heart mitochondria, suggesting that MCJ limits the formation of these supercomplexes. Normally, increased MMP is associated with increased ROS due to the escape of electrons. In contrast, the absence of MCJ increased complex I activity and MMP, but it did not increase ROS. It is possible that the lack of MCJ facilitates the formation of supercomplexes, leading to overall increased complex I activity and MMP but no increase in ROS. In this regard, recent studies have shown that the assembly of complex I into supercomplexes enhances complex I activity (8). We also show here increased complex I activity in supercomplexes in MCJ-deficient mitochondria.

We have previously shown that *MCJ* and *DnaJC15* originated in vertebrates as a result of a gene duplication of *DnaJC19*, another member of the DnaJC family already present in insects (23). The C-terminal region is relatively conserved between MCJ/DnaJC15 and DnaJC19, but unlike MCJ, DnaJC19 lacks an N-terminal region (it has only transmembrane and C-terminal regions). The ortholog of DnaJC19 in yeast is Pam18 (previously named

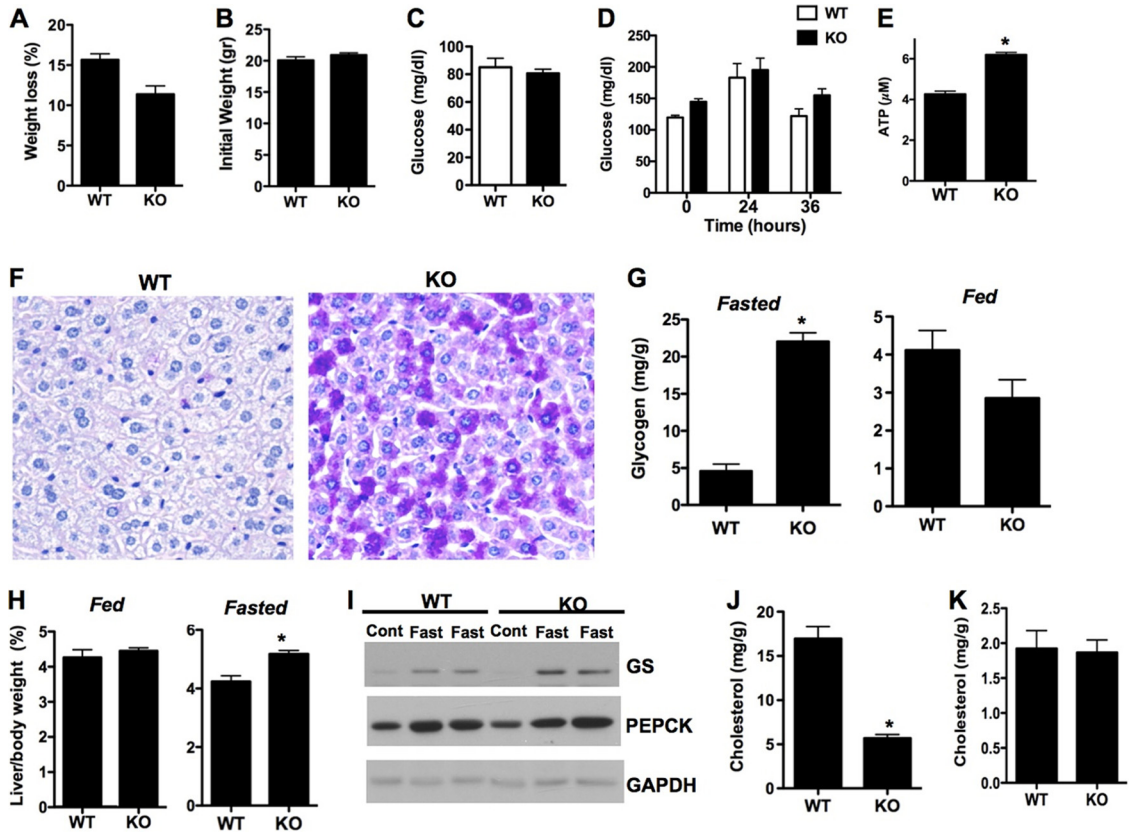

FIG 8 MCJ deficiency promotes glyconeogenesis during fasting. (A) Percentages of total body weight loss after 36 h of fasting relative to the initial weight in WT and MCJ KO mice ($n = 3$). (B) Total body weight in WT and MCJ KO mice prior to fasting. (C) Glucose levels in blood 12 h after fasting. (D) Glucose levels in blood prior to and during fasting. (E) ATP concentrations in liver extracts from WT and MCJ KO mice after fasting (36 h). (F) PAS staining in liver sections from WT and MCJ KO mice after fasting. (G) Glycogen contents in liver extracts from WT and MCJ KO mice ($n = 3$) after fasting (36 h) or normal feeding. (H) Percentages of liver weight versus total body weight in WT and MCJ KO mice after fasting (36 h) or normal feeding. (I) Western blot analysis for glycogen synthase (GS) and PEPCK in livers from WT and MCJ KO mice normally fed (Cont) or after fasting (Fast) for 36 h. Livers from two mice are shown for the fasting condition. (J) Cholesterol content in livers of WT and MCJ KO mice ($n = 5$) after 4 weeks on a high-cholesterol diet. (K) Cholesterol contents in livers of WT and MCJ KO mice ($n = 4$) fed a normal diet. *, $P < 0.05$. Statistical significance was determined by the Student *t* test. The error bars indicate standard deviations.

Tim14), a component of the yeast import motor associated with the inner membrane translocase TIM23, which is involved in the transport of precursor proteins into the mitochondrial matrix (39, 40). In yeast, Pam18 interacts with Pam16, and the heterodimer is required for protein transport into the matrix and for survival of the yeast (41). Interestingly, it has also been reported that both Pam16 and Pam18 interact with the respiratory chain III/IV supercomplexes (yeasts lack complex I) (42). In addition, a recent study in *Drosophila* has reported that Blp, the ortholog of Pam16, also interacts with complex I and complex IV (43). In mammals, DnaJC19 associates with Magmas, the ortholog of Pam16 in mammals, through its C-terminal region and the heterodimer tethered to the translocase (44), but its role in regulating protein transport remains unclear. Based on the conservation of the C-terminal region in DnaJC19 and MCJ/DnaJC15, we found that Magmas also interacts with MCJ by coimmunoprecipitation analyses in mitochondria from mouse heart (data not shown). Furthermore, similar to Blp in *Drosophila*, we also found that Magmas associates with complex I in heart mitochondria (data not shown). These results have been confirmed by a recent study (35). Additional studies will be needed to dissect how MCJ and Magmas may regulate each other and their roles in regulating the translocase-associated motor, as well as the mitochondrial respiratory chain. Blp deficiency has been shown to impair MMP (43), in contrast to MCJ deficiency, which increases MMP. It is possible that these two proteins have opposite roles in mitochondrial respiration. Nevertheless, our studies provide additional evidence for the emerging concept of cross talk between mitochondrial protein transport and mitochondrial respiration.

MCJ appears to be distinct from other members of the DnaJ family identified in mitochondria and is required for mitochondrial function under physiological conditions. In contrast, MCJ is dispensable under normal physiological conditions. This phenotype is compatible with its negative role in mitochondrial respiration, since having an increased metabolism should not be harmful under normal conditions. However, the enhanced mitochondrial function in the absence of MCJ could affect the response and pathology caused by altered metabolic conditions. We demonstrate here that in the absence of the negative regulatory function of MCJ in mitochondria, there is enhanced metabolism of lipids in the liver that minimizes the pathological accumulation of lipids in the liver in response to two opposite altered diets (fasting and high-cholesterol diets). Evolutionarily, the acquisition of MCJ in vertebrates could have been an adaptive phenomenon to deceler-

ate mitochondrial respiration by inhibiting complex I activity in response to insufficient intake of food and to prolong the lipid reserve energy. The rapid loss of fat (both white and brown fat) in MCJ-deficient mice during fasting (data not shown) further supports this hypothesis. Interestingly however, we also observed a marked increase in glycogenesis in the absence of MCJ during fasting, primarily in the liver. This is probably a mechanism of protection for the organism to "store" the excess energy resulting from the enhanced catabolism of fatty acids in the liver. The accumulation of glycogen in the livers of MCJ KO mice during fasting can therefore provide these mice with a source of energy that allows them to maintain their muscle mass intact for a longer time after fat is consumed. Overall, the enhanced mitochondrial metabolism caused by the loss of MCJ can be beneficial in the initial phases of fasting. However, because of the rapid consumption of the available "fuel," we predict that longer fasting periods could be highly detrimental in the absence of MCJ. In contrast, loss of MCJ may be beneficial in reducing accumulation of cholesterol in the liver. It is also possible that the absence of MCJ reduces the accumulation of lipids in the liver under a high fat diet. Oxidation of fatty acids and the metabolic rate have also been found to influence the survival of memory CD8 T cells, with increased mitochondrial fatty acid oxidation correlating with increased survival and function of memory CD8 T cells (45–48). The presence of MCJ in CD8 T cells may be a mechanism to restrain activation of these cells under physiological conditions.

In summary, our studies reveal a novel role of the MCJ/DnaJC15 cochaperone as a negative regulator of mitochondrial respiration by affecting complex I activity and formation of supercomplexes. Importantly, we show for the first time that MCJ/DnaJC15 is essential for attenuating mitochondrial metabolism and that the loss of MCJ modulates the response to altered metabolic conditions. Considering the previously described epigenetic regulation of MCJ expression by methylation, we can speculate that changes in MCJ levels among the human population may account for individual differences in metabolism, primarily in response to major dietary changes, such as high-fat/cholesterol diets or malnutrition. MCJ may also be a potential target to modulate the energy balance.

ACKNOWLEDGMENTS

We thank Marilyn Wadsworth and Nicole Bishop (Microscopy Imaging Center, University of Vermont, Burlington, VT) for help with confocal microscopy and immunoelectron microscopy, Timothy Hunter and Mary Lou Shane (DNA Sequencing Facility, University of Vermont, Burlington, VT) for assistance with real-time RT-PCR analysis, Colette Charland (Flow Cytometry Facility, University of Vermont, Burlington, VT) for help with flow cytometry analysis, Itziar Martín (CIC bioGUNE, Derio, Bizkaia, Spain) for technical assistance, and Sebastian Hasenfuss (CNIO, Madrid, Spain) and Guadalupe Sabio (CNIO) for helpful discussions.

This work was supported by NIH grants CA127099 (M. Rincon), Lake Champlain Cancer Research Organization (M. Rincon), Fundacion Jesus Serra (M. Rincon), AI078277 (J. Anguita), and GM068650 (M. Radermacher).

REFERENCES

1. **Starkov AA.** 2008. The role of mitochondria in reactive oxygen species metabolism and signaling. Ann. N. Y. Acad. Sci. **1147**:37–52.
2. **Cruciat CM, Brunner S, Baumann F, Neupert W, Stuart RA.** 2000. The cytochrome bc1 and cytochrome c oxidase complexes associate to form a single supracomplex in yeast mitochondria. J. Biol. Chem. **275**:18093–18098.
3. **Schagger H, Pfeiffer K.** 2000. Supercomplexes in the respiratory chains of yeast and mammalian mitochondria. EMBO J. **19**:1777–1783.
4. **Stuart RA.** 2008. Supercomplex organization of the oxidative phosphorylation enzymes in yeast mitochondria. J. Bioenerg. Biomembr. **40**:411–417.
5. **Acin-Perez R, Fernandez-Silva P, Peleato ML, Perez-Martos A, Enriquez JA.** 2008. Respiratory active mitochondrial supercomplexes. Mol. Cell **32**:529–539.
6. **Althoff T, Mills DJ, Popot JL, Kuhlbrandt W.** 2011. Arrangement of electron transport chain components in bovine mitochondrial supercomplex I1III2IV1. EMBO J. **30**:4652–4664.
7. **Chen YC, Taylor EB, Dephoure N, Heo JM, Tonhato A, Papandreou I, Nath N, Denko NC, Gygi SP, Rutter J.** 2012. Identification of a protein mediating respiratory supercomplex stability. Cell Metab. **15**:348–360.
8. **Moreno-Lastres D, Fontanesi F, Garcia-Consuegra I, Martin MA, Arenas J, Barrientos A, Ugalde C.** 2012. Mitochondrial complex I plays an essential role in human respirasome assembly. Cell Metab. **15**:324–335.
9. **Vukotic M, Oeljeklaus S, Wiese S, Vogtle FN, Meisinger C, Meyer HE, Zieseniss A, Katschinski DM, Jans DC, Jakobs S, Warscheid B, Rehling P, Deckers M.** 2012. Rcf1 mediates cytochrome oxidase assembly and respirasome formation, revealing heterogeneity of the enzyme complex. Cell Metab. **15**:336–347.
10. **Cairns RA, Harris IS, Mak TW.** 2011. Regulation of cancer cell metabolism. Nat. Rev. Cancer **11**:85–95.
11. **Levine AJ, Puzio-Kuter AM.** 2010. The control of the metabolic switch in cancers by oncogenes and tumor suppressor genes. Science **330**:1340–1344.
12. **Gottlieb RA, Gustafsson AB.** 2011. Mitochondrial turnover in the heart. Biochim. Biophys. Acta **1813**:1295–1301.
13. **Fearnley IM, Carroll J, Shannon RJ, Runswick MJ, Walker JE, Hirst J.** 2001. GRIM-19, a cell death regulatory gene product, is a subunit of bovine mitochondrial NADH:ubiquinone oxidoreductase (complex I). J. Biol. Chem. **276**:38345–38348.
14. **Gough DJ, Corlett A, Schlessinger K, Wegrzyn J, Larner AC, Levy DE.** 2009. Mitochondrial STAT3 supports Ras-dependent oncogenic transformation. Science **324**:1713–1716.
15. **Wegrzyn J, Potla R, Chwae YJ, Sepuri NB, Zhang Q, Koeck T, Derecka M, Szczepanek K, Szelag M, Gornicka A, Moh A, Moghaddas S, Chen Q, Bobbili S, Cichy J, Dulak J, Baker DP, Wolfman A, Stuehr D, Hassan MO, Fu XY, Avadhani N, Drake JI, Fawcett P, Lesnefsky EJ, Larner AC.** 2009. Function of mitochondrial Stat3 in cellular respiration. Science **323**:793–797.
16. **Shridhar V, Bible KC, Staub J, Avula R, Lee YK, Kalli K, Huang H, Hartmann LC, Kaufmann SH, Smith DI.** 2001. Loss of expression of a new member of the DNAJ protein family confers resistance to chemotherapeutic agents used in the treatment of ovarian cancer. Cancer Res. **61**:4258–4265.
17. **Strathdee G, Davies BR, Vass JK, Siddiqui N, Brown R.** 2004. Cell type-specific methylation of an intronic CpG island controls expression of the MCJ gene. Carcinogenesis **25**:693–701.
18. **Ehrlich M, Jiang G, Fiala E, Dome JS, Yu MC, Long TI, Youn B, Sohn OS, Widschwendter M, Tomlinson GE, Chintagumpala M, Champagne M, Parham D, Liang G, Malik K, Laird PW.** 2002. Hypomethylation and hypermethylation of DNA in Wilms tumors. Oncogene **21**:6694–6702.
19. **Lau DT, Hesson LB, Norris MD, Marshall GM, Haber M, Ashton LJ.** 2012. Prognostic significance of promoter DNA methylation in patients with childhood neuroblastoma. Clin. Cancer Res. **18**:5690–5700.
20. **Lindsey JC, Lusher ME, Strathdee G, Brown R, Gilbertson RJ, Bailey S, Ellison DW, Clifford SC.** 2006. Epigenetic inactivation of MCJ (DNAJD1) in malignant paediatric brain tumours. Int. J. Cancer **118**:346–352.
21. **Muthusamy V, Duraisamy S, Bradbury CM, Hobbs C, Curley DP, Nelson B, Bosenberg M.** 2006. Epigenetic silencing of novel tumor suppressors in malignant melanoma. Cancer Res. **66**:11187–11193.
22. **Witham J, Vidot S, Agarwal R, Kaye SB, Richardson A.** 2008. Transient ectopic expression as a method to detect genes conferring drug resistance. Int. J. Cancer **122**:2641–2645.
23. **Hatle KM, Neveu W, Dienz O, Rymarchyk S, Barrantes R, Hale S, Farley N, Lounsbury KM, Bond JP, Taatjes D, Rincon M.** 2007. Methylation-controlled J protein promotes c-Jun degradation to prevent ABCB1 transporter expression. Mol. Cell. Biol. **27**:2952–2966.

24. **Palvinskaya T, Antkowiak M, Burg E, Lenox CC, Ubags N, Cramer A, Rincon M, Dixon AE, Fessler MB, Poynter ME, Suratt BT.** 2012. Effects of acute and chronic low density lipoprotein exposure on neutrophil function. Pulm. Pharmacol. Ther. **17**:S1094–5539(12)00147-2. doi:10.1016/j.pupt.2012.10.002.
25. **Auphan N, Simon AK, Asnagli H, Phillips RJ, Rincón M, Ghosh S, Flavell RA, andSchmitt-Verhulst A-M.** 1998. Consequences of intrathymic TcR engagement by partial agonist on selection events and peripheral T cell activation program. J. Immunol. **160**:4810–4821.
26. **Conze D, Krahl T, Kennedy N, Weiss L, Lumsden J, Hess P, Flavell RA, Le Gros G, Davis RJ, Rincon M.** 2002. c-Jun NH(2)-terminal kinase (JNK)1 and JNK2 have distinct roles in CD8(+) T cell activation. J. Exp. Med. **195**:811–823.
27. **Rincón M, Tugores A, López-Rivas A, Silva A, Alonso M, de Lándazuri MO, López-Botet M.** 1988. Prostaglandin E2 and the increase of intracellular cAMP inhibit the expression of interleukin 2 receptors in human T cells. Eur. J. Immunol. **18**:1791–1796.
28. **Da Cruz S, Xenarios I, Langridge J, Vilbois F, Parone PA, Martinou JC.** 2003. Proteomic analysis of the mouse liver mitochondrial inner membrane. J. Biol. Chem. **278**:41566–41571.
29. **Nubel E, Wittig I, Kerscher S, Brandt U, Schagger H.** 2009. Two-dimensional native electrophoretic analysis of respiratory supercomplexes from Yarrowia lipolytica. Proteomics **9**:2408–2418.
30. **Dudkina NV, Kudryashev M, Stahlberg H, Boekema EJ.** 2011. Interaction of complexes I, III, and IV within the bovine respirasome by single particle cryoelectron tomography. Proc. Natl. Acad. Sci. U. S. A. **108**:15196–15200.
31. **Hamanaka RB, Chandel NS.** 2010. Mitochondrial reactive oxygen species regulate cellular signaling and dictate biological outcomes. Trends Biochem. Sci. **35**:505–513.
32. **Winge DR.** 2012. Sealing the mitochondrial respirasome. Mol. Cell. Biol. **32**:2647–2652.
33. **Teratani T, Tomita K, Suzuki T, Oshikawa T, Yokoyama H, Shimamura K, Tominaga S, Hiroi S, Irie R, Okada Y, Kurihara C, Ebinuma H, Saito H, Hokari R, Sugiyama K, Kanai T, Miura S, Hibi T.** 2012. A high-cholesterol diet exacerbates liver fibrosis in mice via accumulation of free cholesterol in hepatic stellate cells. Gastroenterology **142**:152–164.e10. doi:10.1053/j.gastro.2011.09.049.
34. **Pagliarini DJ, Calvo SE, Chang B, Sheth SA, Vafai SB, Ong SE, Walford GA, Sugiana C, Boneh A, Chen WK, Hill DE, Vidal M, Evans JG, Thorburn DR, Carr SA, Mootha VK.** 2008. A mitochondrial protein compendium elucidates complex I disease biology. Cell **134**:112–123.
35. **Schusdziarra C, Blamowska M, Azem A, Hell K.** 2013. Methylation-controlled J-protein MCJ acts in the import of proteins into human mitochondria. Hum. Mol. Genet. **22**:1348–1357.
36. **McKenzie M, Ryan MT.** 2010. Assembly factors of human mitochondrial complex I and their defects in disease. IUBMB Life **62**:497–502.
37. **Galkin A, Meyer B, Wittig I, Karas M, Schagger H, Vinogradov A, Brandt U.** 2008. Identification of the mitochondrial ND3 subunit as a structural component involved in the active/deactive enzyme transition of respiratory complex I. J. Biol. Chem. **283**:20907–20913.
38. **Maklashina E, Kotlyar AB, Cecchini G.** 2003. Active/de-active transition of respiratory complex I in bacteria, fungi, and animals. Biochim. Biophys. Acta **1606**:95–103.
39. **D'Silva PD, Schilke B, Walter W, Andrew A, Craig EA.** 2003. J protein cochaperone of the mitochondrial inner membrane required for protein import into the mitochondrial matrix. Proc. Natl. Acad. Sci. U. S. A. **100**:13839–13844.
40. **Truscott KN, Voos W, Frazier AE, Lind M, Li Y, Geissler A, Dudek J, Muller H, Sickmann A, Meyer HE, Meisinger C, Guiard B, Rehling P, Pfanner N.** 2003. A J-protein is an essential subunit of the presequence translocase-associated protein import motor of mitochondria. J. Cell Biol. **163**:707–713.
41. **D'Silva PR, Schilke B, Hayashi M, Craig EA.** 2008. Interaction of the J-protein heterodimer Pam18/Pam16 of the mitochondrial import motor with the translocon of the inner membrane. Mol. Biol. Cell **19**:424–432.
42. **Wiedemann N, van der Laan M, Hutu DP, Rehling P, Pfanner N.** 2007. Sorting switch of mitochondrial presequence translocase involves coupling of motor module to respiratory chain. J. Cell Biol. **179**:1115–1122.
43. **Roy S, Short MK, Stanley ER, Jubinsky PT.** 2012. Essential role of Drosophila black-pearl is mediated by its effects on mitochondrial respiration. FASEB J. **26**:3822–3833.
44. **Sinha D, Joshi N, Chittoor B, Samji P, D'Silva P.** 2010. Role of Magmas in protein transport and human mitochondria biogenesis. Hum. Mol. Genet. **19**:1248–1262.
45. **Araki K, Turner AP, Shaffer VO, Gangappa S, Keller SA, Bachmann MF, Larsen CP, Ahmed R.** 2009. mTOR regulates memory CD8 T-cell differentiation. Nature **460**:108–112.
46. **Pearce EL, Walsh MC, Cejas PJ, Harms GM, Shen H, Wang LS, Jones RG, Choi Y.** 2009. Enhancing CD8 T-cell memory by modulating fatty acid metabolism. Nature **460**:103–107.
47. **van der Windt GJ, Everts B, Chang CH, Curtis JD, Freitas TC, Amiel E, Pearce EJ, Pearce EL.** 2012. Mitochondrial respiratory capacity is a critical regulator of CD8(+) T cell memory development. Immunity **36**:68–78.
48. **van der Windt GJ, Pearce EL.** 2012. Metabolic switching and fuel choice during T-cell differentiation and memory development. Immunol. Rev. **249**:27–42.